Journal of Colloid and Interface Science 724 (2026) 141209

Contents lists available at ScienceDirect

Journal of Colloid And Interface Science

journal homepage: www.elsevier.com/locate/jcis

Effect of hydrophilic-lipophilic balance on cavitation-driven emulsification near a liquid-liquid interface

Žan Boček *, Juan Manuel Rosselló, Matevž Dular

Faculty of Mechanical Engineering, University of Ljubljana, Askerceva 6, 1000 Ljubljana, Slovenia

HIGHLIGHTS

- Hydrophilic-lipophilic balance (HLB) value governs cavitation bubble collapse near an oil-water interface.
- Systems with higher HLB values (≥12.9) demonstrate classical cavitation jetting away from the interface.
- Intermediate HLB values (10.7–6.4) produce mixed collapse regimes.
- Systems with low HLB values (4.3) exhibit reversed jetting direction towards the interface.
- Bubble jetting direction determines emulsion type: either oil-in-water (O/W) or water-in-oil (W/O).

GRAPHICAL ABSTRACT

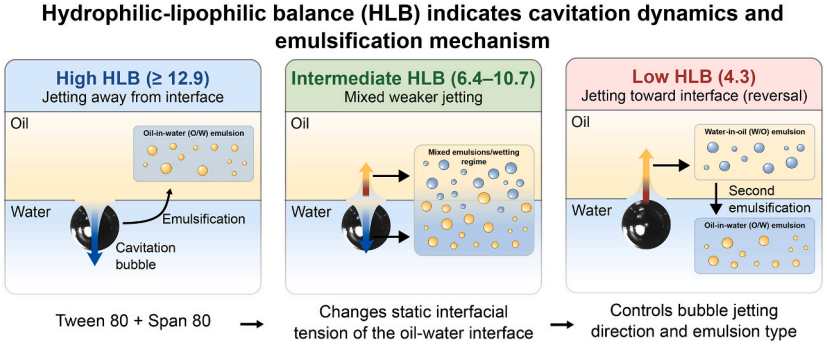

ARTICLE INFO

Keywords:
Cavitation
Single-bubble
Hydrophilic-lipophilic balance
Emulsions
Bubble jetting

ABSTRACT

Hypothesis: Cavitation-driven emulsification is governed by bubble collapse and microjet formation at the liquid-liquid interface, which in turn is correlated with the system's hydrophilic-lipophilic balance (HLB). Modifying the HLB value through the use of surfactants affects interfacial properties, one of which is the static interfacial tension between liquids. This might change emulsification pathways and consequently the type of formed emulsion.

Experiments: The HLB value of an oil-water system was systematically tailored using surfactants Tween 80 and Span 80, which were separately dissolved in demineralized water and silicone oil, respectively. The resulting systems were first characterized in terms of viscosity, surface tension, and static oil-water interfacial tension. Single laser-induced cavitation bubbles were then formed at various distances from the liquid-liquid interface, and their collapse dynamics were characterized using high-speed visualization. Bubble dynamics through bubble centroid displacement were correlated with the HLB value of the respective system.

Findings: In systems with higher HLB values (≥ 12.9), bubbles always collapsed away from the oil-water interface, following classical density-driven jetting behaviour. Intermediate values (between 10.7 and 6.4) produced bubble collapse both towards and away from the interface. At the lowest HLB value of 4.3, bubbles collapsed towards the oil-water interface, a reversal of the expected jetting direction. These indicate different emulsification pathways, which are consistent with typical HLB ranges for surfactant applications. This demonstrates that

* Corresponding author.
E-mail address: zan.bocek@fs.uni-lj.si (Ž. Boček).

https://doi.org/10.1016/j.jcis.2026.141209
Received 17 March 2026; Received in revised form 17 June 2026; Accepted 23 July 2026
Available online 28 July 2026

in cavitation-driven emulsification, the system's HLB value affects directly the collapse dynamics of cavitation bubbles, and consequently, the type of emulsion they produce.

1. Introduction

Emulsions are colloidal systems consisting of two immiscible liquids, typically oil and water. Their unique property is that one liquid is dispersed inside the other in the form of variously sized droplets [1]. This enables the combination of otherwise immiscible liquids and results in products with enhanced stability [2,3], improved texture [4–6] or the ability for controlled release of active ingredients [7–10]. Emulsions consequently perform key functions in industries ranging from food and cosmetics to pharmaceuticals and energy applications [11,12].

As great amounts of energy are required for the dispersion of droplets into fine emulsion, alternative low-energy techniques are continuously being explored. Such an approach is with the use of cavitation [13]. This is the appearance of vapor cavities inside a liquid medium due to an extreme local pressure drop [14]. When the gas pressure inside the bubble then drops below that of the ambient liquid, the cavity undergoes an inertial collapse [14,15]. Great amounts of energy are released in the process, which disrupts the liquid-liquid interface, promotes droplet dispersion and accelerates mass transfer [16–20]. Combined with its lower energy intensity compared to conventional homogenization techniques (e.g. high-pressure and rotor-stator homogenizers), cavitation presents a promising alternative to classical emulsification techniques [13,17]. The latter are unable to create physical conditions intense enough for the formation of nanoemulsions [2,12,13].

Depending on the surrounding medium's boundary conditions, cavitation bubble collapse might either be spherically symmetrical or nonspherical [14]. In the latter case, a high-speed microjet forms, always pointing towards the denser phase of a liquid-liquid interface [16,21]. Collapsing near solid boundaries, bubbles jet towards the boundary due to pressure asymmetries [22]. Collapsing near free boundaries, however, the bubble jetting is directed away from the boundary, with the boundary absorbing energy and deforming [23–25].

Nonspherical bubble collapse near a liquid-liquid interface, especially the formation of a high-speed microjet, greatly facilitates the emulsification of liquids and directly determines the type of formed emulsion [16,17]. Bubble collapse inside the water phase away from the interface will namely promote the formation of O/W emulsions. During bubble oscillation and finally its collapse, segments of the oil phase will be pulled into the water phase [17–19,21]. This protruding segment will then separate from the bulk and disperse into small droplets, resulting in emulsion formation.

On the other hand, if such a bubble collapses and jets towards the interface, this promotes the formation of W/O emulsion. The bubble creates a water protrusion into the oil phase, which similarly detaches from the bulk and separates into finer droplets, creating droplets of W/O emulsion [19–21,26–28]. In both cases, however, emulsion formation is not limited to only one type, with different types forming simultaneously. Fluid instabilities additionally contribute to emulsification [17]. In case of cavitation bubble collapse inside the oil phase, classical bubble dynamics dictate jetting towards the oil-water interface [19,21,29,30]. This results in the formation of O/W emulsions [16,17,20,26]. Based on emulsification behaviour of cavitation bubble collapse inside the water phase, bubble jetting inside the oil phase away from the oil-water interface would be expected to form W/O emulsion. However, such phenomena have, to our knowledge, not yet been reported [16–20,26,27,29,30].

Because emulsions are thermodynamically unstable systems, surface active agents (surfactants) are commonly added during their preparation to improve stability and control droplet formation [31]. Surfactants reduce surface and interfacial tension, as well as modify the interfacial rheology of liquids [21,31]. Thereby, they facilitate droplet breakup and prevent coalescence. As emulsions without added surfactants exhibit relatively bad stability and larger average droplet sizes [2,31–33], the inclusion of surfactants is crucial for the preparation of emulsion with required physical properties.

Surfactant molecules contain a hydrophilic and a lipophilic segment, enabling absorption at the oil-water interface. The relative affinity of a surfactant for either water or oil is quantified by its hydrophilic-lipophilic balance (HLB). It typically ranges from 0 to 20, with higher HLB values indicating stronger hydrophilicity and generally associated with O/W emulsions. Lower values indicate greater lipophilicity and favour W/O emulsions. In a blend of surfactants, the HLB value of the system is additive and can therefore be tailored to the desired emulsification characteristics.

For emulsion preparation, the HLB value of a surfactant or system of surfactants is chosen based on the desired application. For W/O emulsions this range is usually between 3 and 6 [32,34,35], sometimes also defined from 3 to 8 [36,37] or simply below 7 [33]. On the other hand, surfactants for the preparation of O/W emulsion usually range from 8 to 16 [32] or 18 [34,35]. They are also sometimes identified as ranging from 9 to 12 [36,37] or simply above 7 [33]. Surfactants with HLB values from 7 to 9, partially overlapping with other emulsification ranges, are used as wetting agents [34,35]. Rather than forming stable O/W or W/O emulsions, these promote the wetting of surfaces, i.e. the spreading of one phase over another or a solid surface [38–40].

The cavitation bubble collapse dynamics near liquid-liquid interfaces have already been previously studied. The cavitation bubble collapse dynamics near liquid-liquid interfaces were studied in the present work. Recent research has used high-speed imaging and numerical investigations to clarify the role of density gradients, viscosity variations and interface deformability on bubble collapse asymmetry, jetting direction and rebound properties [19,21,29,30]. Regarding emulsion formation, these studies focused on microjet contribution to emulsification mechanisms: interface disruption, mass transfer improvement and droplet entrainment [16–20,26–28]. The present work aims to demonstrated that interfacial properties could alter collapse anisotropy and modify microjet penetration dynamics near soft or free surfaces [20,23–25,28]. However, the influence of surfactant properties and especially the HLB value on bubble collapse behaviour remains unexplored in literature. Surface and interfacial tension strongly affect bubble dynamics and jetting [41–43]. Through this, the HLB value of a system [35] is expected to crucially modify cavitation-driven emulsification. Such an investigation linking HLB-tailored interfacial properties with single-bubble collapse dynamics is still lacking.

The present study aims to explore the effect HLB value has on cavitation bubble collapse at various distances from a liquid-liquid interface. Two commonly used surfactants, Tween 80 and Span 80, have been employed to adjust the systems HLB value by varying their ratios. Firstly, the effect of surfactant addition on the physical properties of oil and water has been studied. This was done to determine the cause for changing bubble collapse dynamics. High-speed imaging has then been used to characterize bubble collapse direction and magnitude of displacement.

2. Experimental method

2.1. Surfactant solution preparation

The HLB value of the oil-water system was modified with the addition of surfactants Polyoxyethylene Sorbitan Monooleate (Tween 80, CAS No. 9005-65-6, Tokyo Chemical Industry, Japan) and Sorbitan monooleate (Span 80, CAS No. 1338-43-8, Tokyo Chemical Industry,

Japan). They were chosen due to their widespread use in literature [7–9] and well understood physical and chemical properties [31,32].

They were diluted separately in demineralized water (dH_2O) and silicone oil (SiOil), respectively. The SiOil (CAS No. 63148–62-9, Sigma-Aldrich, Germany) had a density of 0.967 g/mL (at 20 °C). The combined volumes of Tween 80 and Span 80 always represented 8 vol% of the oil-water system.

The surfactant ratios (concentrations) were chosen based on the desired HLB value of the system (Table 1). These were 15.0 for exclusively Tween 80 and 4.3 for exclusively Span 80, with four equally spaced values in-between: 12.9, 10.7, 8.6 and 6.4. These HLB values were chosen to evenly span the blending interwall between pure surfactants, as the cavitation bubble collapse dynamics were initially expected to change proportionally to the system's HLB value. The required Tween 80 to Span 80 ratios for the desired HLB values were calculated based on the following Eq. [13]:

$$HLB_{desired} = \varphi_{Tween\ 80} \cdot HLB_{Tween\ 80} + \varphi_{Span\ 80} \cdot HLB_{Span\ 80} \quad (1)$$

Here $\varphi_{Tween\ 80}$ and $\varphi_{Span\ 80}$ represent the volume fractions of Tween 80 and Span 80, respectively, with $HLB_{Tween\ 80}$ and $HLB_{Span\ 80}$ being the HLB values of their respective pure surfactants. The control sample (∞) of pure dH_2O and SiOil contained neither surfactant. Tween 80 and Span 80 dissolution was improved by heating the solutions in a water bath to 50 °C and stirring with a vortex mixer for approximately 2 h. The solutions were additionally stirred for up to 15 min immediately before measurements. Tween 80 completely dissolved in dH_2O at all concentrations, resulting in a clear, slightly darker liquid. Meanwhile, Span 80 only partially dissolved in the SiOil, forming a milky solution with high opacity.

The HLB values of the surfactant ratios were estimated through emulsion stability experiments (data not shown). Using the corresponding dH_2O-Tween 80 and SiOil-Span 80 solutions from Table 1, emulsion were prepared with an UP200St ultrasonic horn (Hielscher, Germany). It operated at 26 kHz and 20% amplitude for 10 min for the preparation of each emulsion. The highest stability was noted in systems with suspected HLB values of 10.7 and 12.9. As greater emulsion stability is linked to lower average droplet size, this indicates the oil-water system's optimal HLB value [44]. Such HLB corresponds to optimal values of similar emulsion systems [45]. This indicates the suitability of the presented HLB tailoring method in preparing expected HLB values.

2.2. Dynamic viscosity measurements

Dynamic viscosity measurements (μ) of the dH_2O-Tween 80 and SiOil-Span 80 solutions were conducted using a Physica MCR 301 rotational rheometer (Anton Paar, Austria) at 25 °C. The instrument was equipped with a standard double-gap measuring system (C-DG26.7/T200, Anton Paar, Austria). The viscosities were measured under steady shear flow ranging from 0.01 to 1000 s^{-1}. To ensure data reliability, each sample was measured at least thrice.

Table 1
Tween 80 and Span 80 concentrations dissolved in demineralized water (dH_2O) and silicone oil (SiOil), respectively, for the preparation of the HLB-tailored systems. Densities were calculated based on surfactant concentrations and the densities of pure components.

HLB [/]	Tween 80: Span 80	c(Tween 80) [vol% in dH_2O]	c(Span 80) [vol% in SiOil]	ρ(dH_2O-Tween 80) @20 °C [g/mL]	ρ(SiOil-Span 80) @20 °C [g/mL]
∞[1]	/	/	/	1.000	0.967
15.0	1:0	8.0	/	1.006	0.967
12.9	4:1	6.4	1.6	1.005	0.967
10.7	3:2	4.8	3.2	1.004	0.968
8.6	2:3	3.2	4.8	1.003	0.968
6.4	1:4	1.6	6.4	1.001	0.968
4.3	0:1	/	8.0	1.000	0.969

[1] Pure dH2O and SiOil without the addition of either surfactant.

2.3. Surface and static interfacial tension measurements

The static surface (liquid-air interface) tension (σ_s) of each dH_2O-Tween 80 and SiOil-Span 80 solution was individually measured. Furthermore, static interfacial tension (σ_i) measurements at the liquid-liquid interface were performed for each HLB-tailored system. Both measurement types were done using an EZ-Pi Plus tensiometer (Kibron, Finland) and the de Noüy ring method at 25 °C. The mean and standard deviation values for each sample were calculated from a minimum of 3 independent measurements.

2.4. Cavitation bubble formation and visualization setup

Cavitation bubbles were produced near the oil-water interface inside a purposely made cuvette (Fig. 1a) using a Nd:YAG laser (Nano Series, Litron Lasers, United Kingdom) emitting at a wavelength of 532 nm. Laser intensity measured over 30 pulses was 553 μJ with a standard deviation of 18 μJ. The laser light of a single pulse was focused to a single point in the middle of the cuvette using a 10× L Plan objective. The resulting bubbles had an average diameter of 1.04 ± 0.06 mm.

The cuvette consisted of a 3D printed base and top, with notches for the four transparent sides made from 2 mm thick polycarbonate. These were sealed to the 3D printed parts and each other with epoxy. The inside dimensions (D × W × H) of the cuvette were approximately 18 × 18 × 24 mm. Polycarbonate was chosen due to the low static contact angle it forms with the oil-water interface [27,46]. The dH_2O-Tween 80 solution was added to the cuvette through a syringe connected to its bottom. Using a micropipette, 2 mL of the SiOil-Span 80 solution were then carefully deposited on top. The oil-water interface position could be adjusted by changing the amount of dH_2O-Tween 80 solution [27].

Due to the high opacity of the SiOil-Span 80 solutions, the formation of cavitation bubbles was limited to the denser dH_2O-Tween 80 solutions. The exact oil-water interface height was set with a micro positioning system moving the whole cuvette. The relative distance between the initial bubble centre and interface (dimensionless standoff parameter γ_0) varied from 0.1 to 3.0 and was defined as:

$$\gamma_0 = h/R_{max} \quad (2)$$

where h represents the distance between the bubble centre and the oil-water interface, and R_{max} the maximum bubble radius (Fig. 1b) [47].

A Kirana 7M (Specialised Imaging, United Kingdom) high-speed camera was used for the visualization of cavitation bubble collapse. For statistical evaluation of bubble collapse, the high-speed camera operated at 250 k frames per second, a shutter speed of 4 μs and was equipped with an M Plan 5X objective (Mitutoyo, Japan). For more detailed visualization of bubble collapse dynamics and emulsification, the camera was equipped with an M Plan 20× objective (Mitutoyo, Japan). It operated at 1 million frames per second, 1 μs shutter speed and 100 k frames per second, 1.5 μs shutter speed, respectively.

Illumination was provided by two custom made LED lights. One was positioned directly opposite the high-speed camera behind the cuvette (Fig. 1a). Depending on the required illumination intensity as dictated by the high-speed cameras shutter speed, it operated at either 8.6 or 12 W. The second LED light (operating at 61 W) was offset from the first approximately 30° both vertically and horizontally (Fig. 1a), illuminating the bubble and interface simultaneously from below and from the side.

The resulting visualization data was analysed by manually determining the initial bubble centre position, its maximum radius (R_{max}), centre of the first rebound bubble and the oil-water interface position (Fig. 1b). The latter was determined by determining the highest position, where the bubble still consistently formed. From these, we calculated

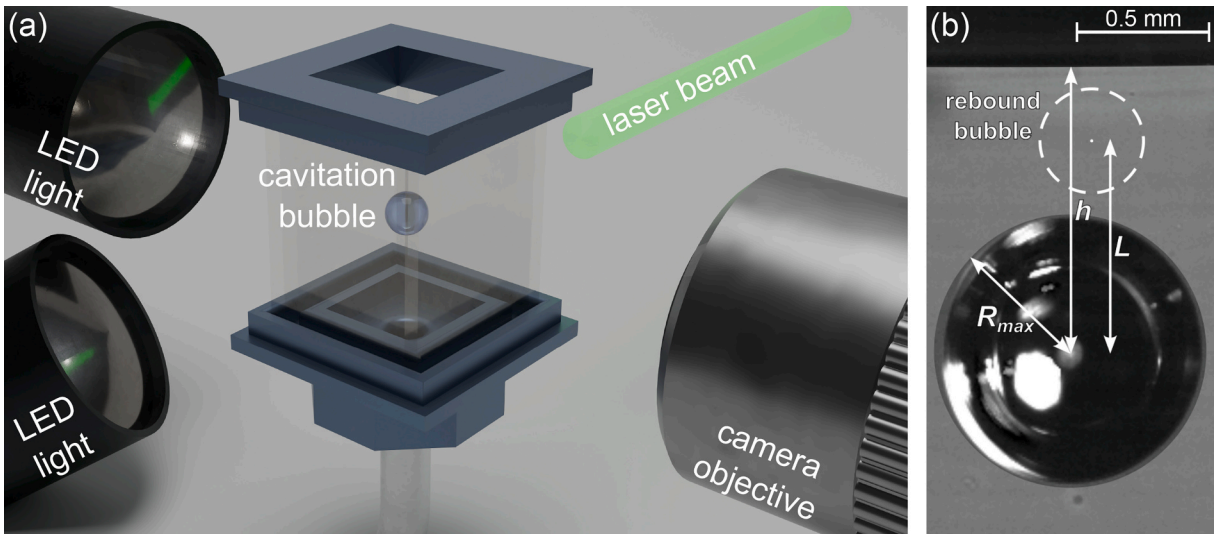

Fig. 1. (a) Experimental setup for single cavitation bubble formation and high-speed visualization (the green line indicates laser beam path, cavitation bubble not to scale) and (b) example of visualization data analysis: maximum bubble radius (R_{max}), bubble centre to oil-water interface distance (h), and vertical bubble centroid displacement from the initial to the first rebound bubble (L). (For interpretation of the references to colour in this figure legend, the reader is referred to the web version of this article.)

the γ_0 values, as well as the vertical displacement to the first rebound bubble relative to the initial bubble's maximum radius (L/R_{max}). Bubble and interface parameter measurements resulted in a maximum measurement uncertainty of approx. 3% for L/Rmax and 7% for γ0. Higher uncertainty of the letter is due to the diffuse oil-water interface at higher Span 80 concentrations.

3. Results and discussion

3.1. Surfactant influence on viscosity and surface tension

Prior to cavitation bubble collapse visualization, the physical properties of the prepared surfactant solutions have been studied. These include dynamic viscosity (μ) and surface tension (σ_s) of individual dH_2O-Tween 80 and SiOil-Span 80 solutions, which are presented Fig. 2. Alongside, static interfacial tension (σ_i) between corresponding dH_2O-Tween 80 and SiOil-Span 80 solutions was measured. Its influence, along with that of individual surface tensions, on cavitation bubble collapse dynamics is discussed in Section 3.4.

Calculations of the solutions' densities (Table 1) show that the addition of surfactant to either dH_2O or SiOil has a negligible effect. The density ratio, which strongly affects the volume and kinetic energy of bubble jetting, is always maintained [21]. Due to the increased opacity of the SiOil-Span 80 solutions, cavitation bubbles could only be formed inside the (denser) dH_2O-Tween 80 phases. According to the anisotropy parameter [47], the bubbles would thus always be expected to jet and collapse away from oil-water interface.

Viscosity measurements of the dH_2O-Tween 80 solutions (Fig. 2a) revealed a gradual increase in viscosity with an increase in HLB value. For these samples, the HLB value and Tween 80 concentration are proportional. The observed increase in viscosity is due to strong interactions between the hydrophilic parts of Tween molecules and water, which alters water structure and increases its resistance to flow [48,49]. Hence, the solution with the highest HLB value of 15.0 also had the

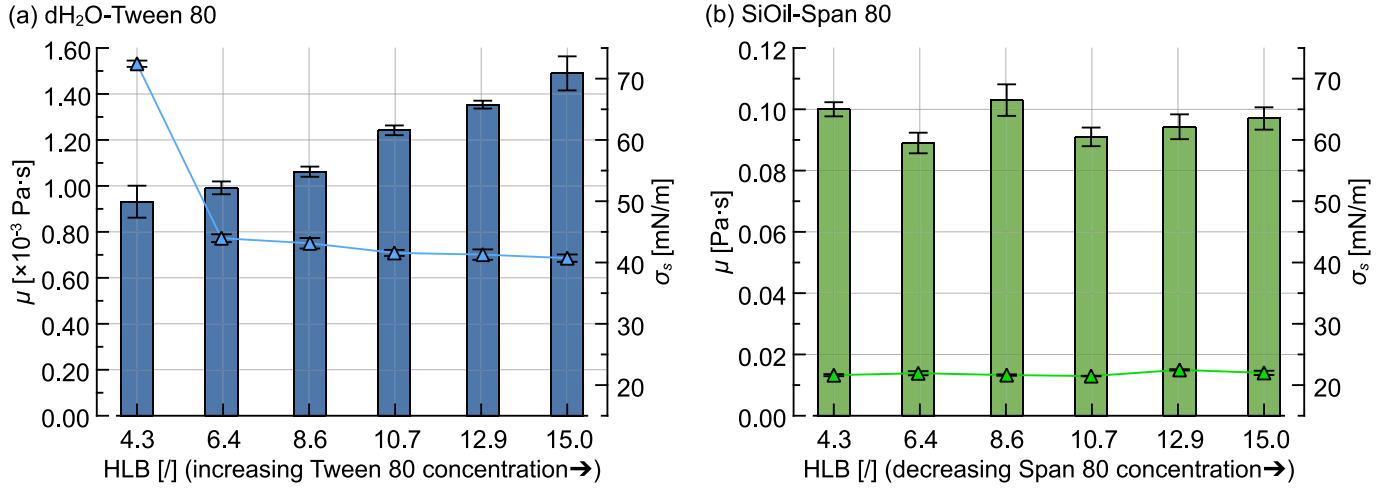

Fig. 2. Results of dynamic viscosity (μ) and surface tension (σ_s) measurements at 25 °C: (a) demineralized water (dH_2O)-Tween 80 and (b) silicone oil (SiOil)-Span 80 solutions. The bars represent viscosity and ▲ surface tension. The average and standard deviation data was calculated from three independent measurement repetitions. In the dH_2O-Tween 80 solutions surfactant concentration increases with hydrophilic-lipophilic balance (HLB) value and in the SiOil-Span 80 solutions it decreases with HLB. The data at HLB values of 4.3 and 15.0 represent pure dH_2O and SiOil, respectively.

highest viscosity at 1.49 × 10^{-3} Pa·s.

SiOil-Span 80 measurements (Fig. 2b) on the other hand revealed no trends in viscosity based on changing HLB/Span 80 concentration. The addition of surfactants was reported to affect oil viscosity due to surfactant-oil molecular interactions [50,51]. However, the used concentrations (≤ 0.15 vol%) were much lower compared to the here presented results. Differences in measured viscosity between pure SiOil at HLB 15.0 (0.097 Pa·s) and SiOil with the highest concentration of Span 80 at HLB 4.3 (0.100 Pa·s) were thus negligible. These, together with the deviations at intermediate concentrations, can be attributed to incomplete Span 80 dissolution inside SiOil. Nevertheless, neither variations in dH_2O-Tween 80 nor SiOil-Span 80 viscosities were high enough to influence cavitation bubble dynamics. Previous research has shown that multiples increase in viscosity is required for it to affect bubble dynamics [19,52–54].

Similarly to viscosity, the surface tension of dH_2O-Tween 80 solutions was also found to change proportionally to HLB value/surfactant concentration (Fig. 2a). The lowest addition of Tween 80 already led to a great decrease in average surface tension compared to that of pure dH_2O: from 72.4 to 44.0 mN m^{-1}, respectively. The surfactant absorbs strongly to the liquid-air interface even at low concentrations. Here it replaces surface water molecules, reducing the formation of stronger intermolecular forces [55,56]. Further increase in concentration caused a steady decrease in surface tension due to increased surfactant adsorption to the interface and changed molecular orientation [31,57–59]. It thus reached its lowest value of 40.7 mN m^{-1} at HLB 15.0.

No direct correlation between Span 80 concentration and SiOil surface tension was observed (Fig. 2b). The overall standard deviation of all measurements was found to be 0.4 mN m^{-1}, with pure SiOil (at an HLB of 15.0) having an intermediate surface tension compared to other solutions. Surfactants generally have a similar effect on the surface tension of oils as they do on water. By absorbing to the surface, they decrease interfacial free energy [60,61]. As with viscosity, the lack of surfactant influence on surface tension is potentially due to its high concentration. This exceeded its critical micelle concentration [60], where surfactant molecules form micelles instead of dissolving in the liquid. The critical micelle concentration of Span 80 is much lower compared to that of Tween 80 [62].

3.2. Bubble collapse visualization

Fig. 3 presents examples of cavitation bubble collapse dynamics for systems with HLB values of 15.0, 8.6 and 4.3. These illustrate the three characteristic bubble jetting cases: strongly (Fig. 3a) and weakly (Fig. 3b) away from the oil-water interface, as well as towards it (Fig. 3c). The frames are timed relative to the bubble growing to its maximum radius (t_0), with the leftmost frame showing the initial oil-water interface. Low dimensionless standoff parameters (γ_0) were used to maximize the interface's effect on bubble collapse. The upper phase is always SiOil and the lower dH_2O.

In case of an HLB value of 15.0 (Fig. 3a) and 8.6 (Fig. 3b), the bubble was found to jet away from the oil-water interface. This is in accordance with previous research [27,29,30,47,63], which found that a bubble formed inside the denser liquid (dH_2O-Tween 80) jets away from the liquid-liquid interface. With the higher HLB value, a strong jet was clearly visible as it penetrated through the bubble and pinched off. Jetting in the system with an HLB value of 8.6 was found to be weaker. No jet exiting the bubble was observed, only an indentation of the bubble part furthest away from the oil-water interface. However, a jet is briefly visible inside the bubble (Fig. 3b, 8th frame).

Bubble parts closer to the boundary, in this case the oil-water interface, contract faster (Fig. 3a, 2nd frame). This causes the formation of a high-pressure point in that area, together with the emergence of a high-speed microjet. The latter points towards the low-pressure region, i.e. the part of the bubble furthest away from the interface [16,23,64]. The anisotropy of the resulting pressure field is greater at lower initial bubble-interface distances, simultaneously resulting in stronger jetting [27,29,54,64,65]. As the bubble continues to collapse, it is penetrated by the high-speed jet. With this, the bubble becomes elongated and is displaced in the direction of jetting [22,27,29,66].

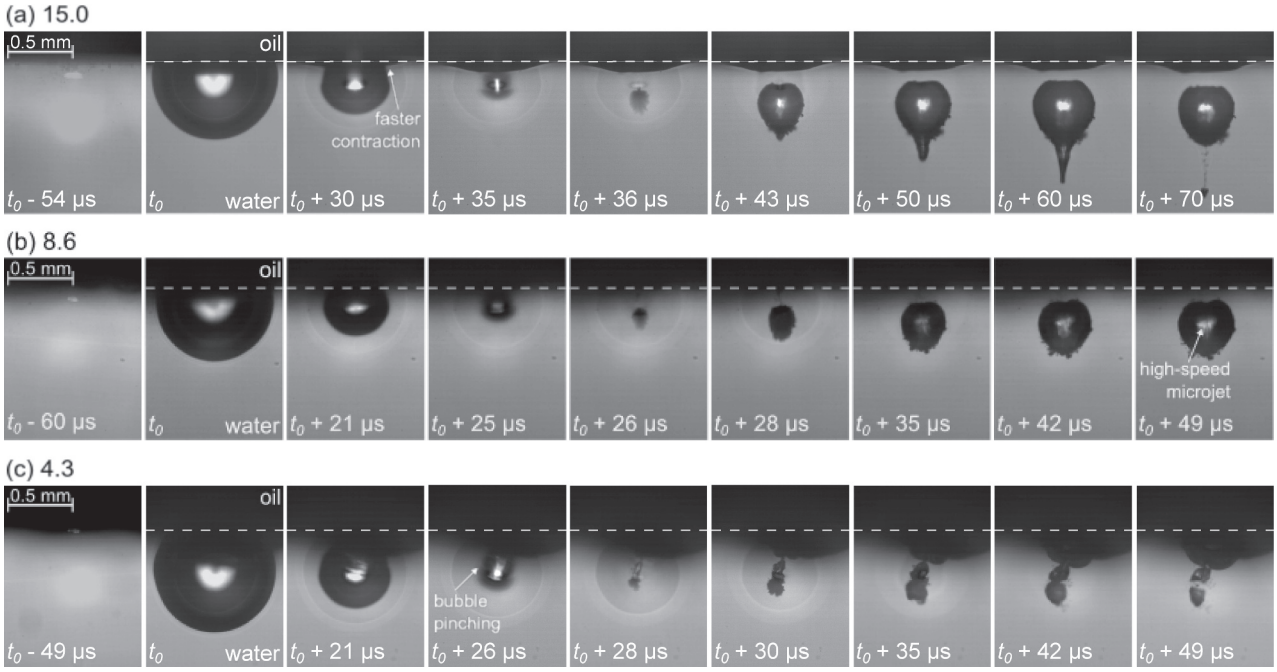

Fig. 3. (videos S1–S3 in Supplementary material): Sequences showing cavitation bubble jetting due to proximity of the oil-water interface for chosen hydrophilic-lipophilic balance (HLB) values: (a) 15.0, (b) 8.6 and (c) 4.3. Their dimensionless standoff parameters (γ_0) were 0.22, 0.24 and 0.67, respectively. The visible bubble artifacts are due to the camera ghosting effect. The white dashed lines represent the respective oil-water interface position. Frames are presented from maximum bubble growth to jet formation. At an HLB value of 15.0 the bubble distinctly jets away from the interface and at 4.3 towards it. At 8.6 HLB a weaker jet forms away from the interface.

In the system with the lowest HLB value of 4.3 (Fig. 3c) the bubble was observed to jet towards the oil-water interface. Due to uneven collapse, the bubble begins to pinch in its middle (Fig. 3c, 3rd frame) and separates into multiple parts. This causes it to collapse into a linear shape, which points towards the interface. During the following growth, individual segment grew into separate bubbles, with the largest almost completely penetrating through the interface. Due to the uneven oil-water interface, the bubble jetting was slightly tilted. With a decreasing HLB value of the system (decreasing Tween 80 and increasing Span 80 concentration, Table 1) the oil-water interface became less distinct. Higher Span 80 concentrations result in continuously greater hydrophilic-lipophilic imbalance, which leads to weaker and less organized packing of surfactant molecules on the interface [67].

Such variations in bubble collapse behaviour as seen on Fig. 3 can most likely not be attributed to the system's acoustic impedance as it does not affect jet velocity or its direction during bubble collapse. It can, however, alter the propagation or reflection of shockwaves [68]. Nonetheless, the difference in acoustic impedance between materials composing the interface must be significant (i.e. a solid-liquid boundary). Due to the small difference in acoustic impedance of the oil and water phases, the shockwave will mostly propagate through the interface without influencing subsequent bubble dynamics. Furthermore, the minimal differences in solution densities (Table 1) would have negligible effects on the speed of sound within them and as such on their acoustic impedance [69]. The spherical nature of the acoustic wavefront would also result in the reflected waves propagating away from the cavitation bubble. This would reduce the amplitude of the rebound pressure front on the bubble.

Fig. 4 presents cavitation bubble displacement during collapse for the oil-water system with an HLB value of 4.3. Similar examples for the other systems can be found in the Supplementary material section. The key frames show the initial bubble at maximum radius, its collapse and the first rebound bubble at maximum radius. The examples were chosen to illustrate bubble displacement at major values of the dimensionless standoff parameter (γ_0): approximately 0.1, 0.5, 1.0, 1.5 and 2.0. The upper phase is always SiOil and the lower dH_2O. On the top right of each sequence is the calculated bubble centroid displacement up to the first rebound bubble (L/R_{max}). Negative values indicate bubble displacement away from the interface and positive values towards it.

The aforementioned system contained the highest Span 80 concentration, without any Tween 80. It exhibited completely unique bubble collapse dynamics compared to the higher HLB systems (Fig. S4 and S5 in Supplementary material). At the highest initial bubble-interface distance ($\gamma_0 \approx 2.0$) the bubbles collapsed away from the oil-water interface. Down to $\gamma_0 \approx 1.5$, the magnitude of bubble displacement sharply decreased, resulting in almost stationary collapse. These changes in collapse direction and magnitude continued with decreasing γ_0. Bubble displacement around $\gamma_0 \approx 1.0$ and 0.5 was distinctly oriented towards the interface, with its magnitude being highest at $\gamma_0 \approx 0.5$. However, at the shortest initial bubble-interface distance ($\gamma_0 \approx 0.1$) the magnitude of bubble displacement decreased. The latter can be attributed to a greater influence of the interface on bubble collapse dynamics at shorter distances.

3.3. Bubble displacement calculations

Fig. 5 displays the bubble centroid displacement (L/R_{max}) as a function of the dimensionless standoff parameter (γ_0) for each measurement. Displacement was calculated as the distance between initial and first rebound bubble centre (both at maximum radius), divided by the initial bubble's maximum radius. Negative values represent bubble movement away from the oil-water interface and positive values towards it. The dashed lines visualize trends in bubble collapse dynamics. They have been calculated by fitting second-degree exponential functions to the bubble centroid displacement results of individual dH_2O-SiOil systems. This fit is empirical and does not represent a physically

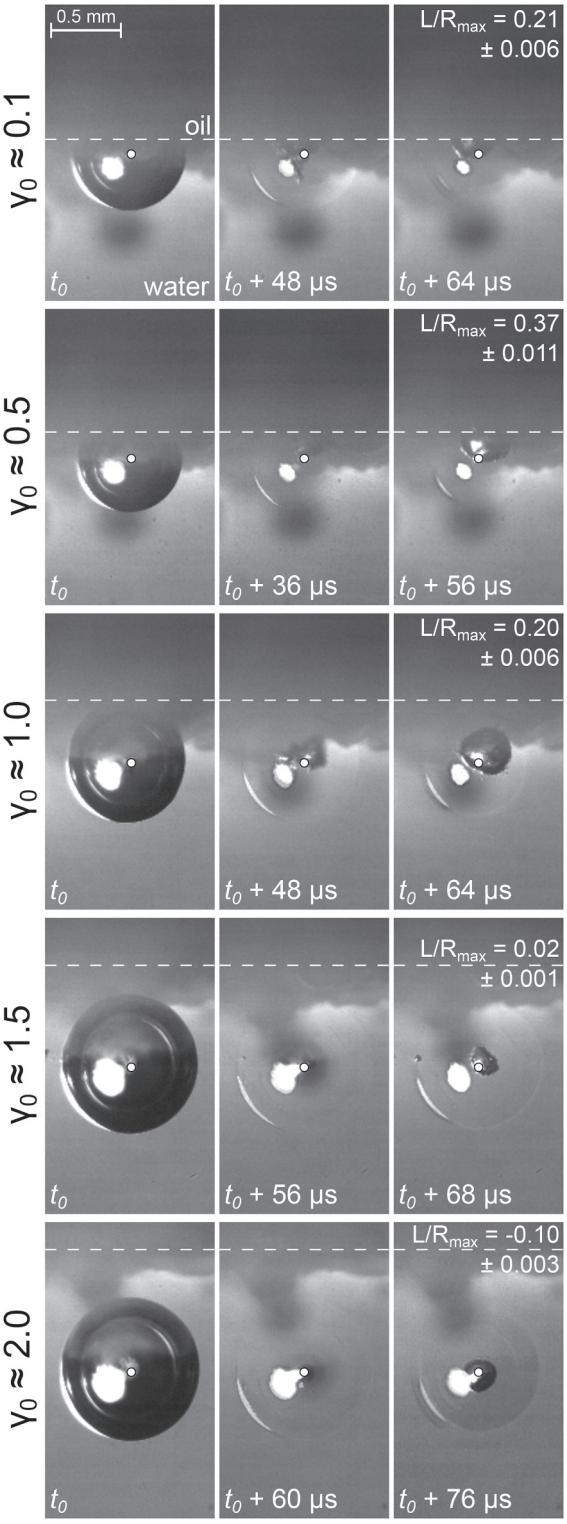

Fig. 4. Sequences of cavitation bubble collapse near the oil-water interface at a hydrophilic-lipophilic balance (HLB) value of 4.3. The bubble artifacts visible on frames two and three of each sequence are due to the camera ghosting effect. The white dashed lines represent the oil-water interface position and the white dots the initial bubble's centre. The frames show the initial bubble at maximum radius, the bubble during collapse and the first rebound bubble at maximum radius. Examples are presented at approximate dimensionless standoff parameters (γ_0) 0.1, 0.5, 1.0, 1.5 and 2.0. On the top right corner of each sequence are the calculated values of bubble centroid displacement (L/R_{max}) together with the estimated deviations.

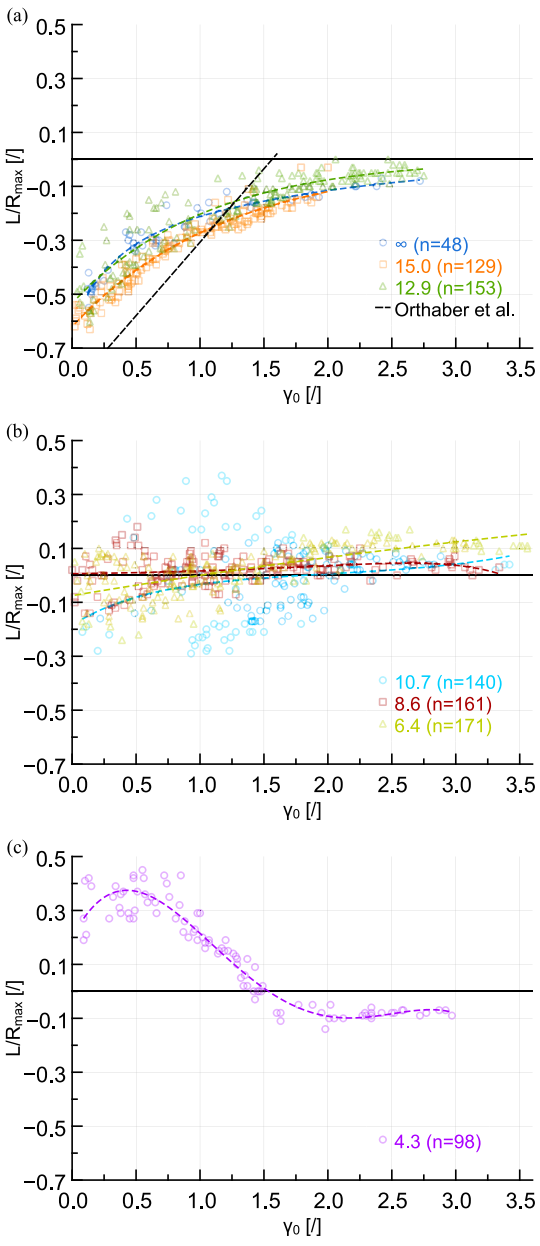

Fig. 5. Cavitation bubble centroid displacement during collapse relative to its maximum radius (L/R_{max}) as a function of the dimensionless standoff parameters (γ_0). Samples are grouped based on hydrophilic-lipophilic balance (HLB) value: (a) ∞ (demineralized water and silicone oil without any surfactant), 15.0, 12.9, (b) 10.7, 8.6, 6.4 and (c) 4.3. Negative L/R_{max} values indicate bubble centroid displacement away from the oil-water interface (and vice versa). Values next to the labels represent the number of samples analysed for each system. The L/R_{max} and γ_0 values have a measurement uncertainty of approx. 3% and 7%, respectively. The black dashed line in (a) shows experimental data acquired by Orthaber et al. [27].

based model. It is instead used for facilitating the visualization of data trends. The equation, as well as its parameters and fitting degree are included in S6 of the Supplementary material.

Due to the low measurement uncertainty of the calculated L/R_{max} values (≈ 3%), their impact on bubble centroid displacement trends is estimated to be negligible, not affecting the measured displacement directions. As L/R_{max} is not directly calculated from γ_0, the measurement uncertainty of the latter (≈ 7%) has no effect on the calculated trends. Samples are grouped based on similar effects changing γ_0 has on centroid displacement during collapse. The values next to the labels in the legend represent the number of measurements for each oil-water system.

Bubble collapse dynamics in systems with HLB values of 15.0 and 12.9 were found to be similar to the dH_2O and SiOil system without any added surfactant. Regardless of γ_0, the bubbles always collapsed away from the interface (Fig. 5a). Due to the greater interface influence, larger displacement occurred at lower γ_0. These systems displayed low data dispersion. Individual measurements overlapped significantly and deviated relatively little from the calculated trendlines. This is maintained regardless of initial bubble-interface distance. Data obtained by Orthaber et al. [27] is included in Fig. 5a to compare our results with literature. Using a dH_2O-SiOil system without surfactant they found similar trends in collapse dynamics where bubble displacement increases with decreasing γ_0. They, however, fitted a linear trend to the measurements.

Systems with HLB values of 10.7, 8.6 and 6.4 all exhibited bubble collapse both towards and away from the oil-water interface, as well as in place (Fig. 5b). At γ_0 values of ≈ 2.0 and 1.5 the bubbles, although formed inside the denser dH_2O-Tween 80 phase, predominantly collapsed towards the oil-water interface. This contradicts bubble collapse dynamics of the higher HLB examples, as well as observations from literature [29,30,63]. With decreasing initial bubble-interface distance ($\gamma_0 \approx 1.0$), the average bubble displacement decreased to nearly in-place collapse. In the system with an HLB of 8.6 bubble displacement remained roughly constant afterwards, fluctuating around zero. Meanwhile in the 10.7 and 6.4 HLB systems, bubble collapse distinctly favoured displacement away from the interface. This increased in intensity with decreasing γ_0.

Individual measurements for systems with HLB values of 10.7, 8.6 and 6.4 (Fig. 5b) were also more dispersed, overlapping less and deviating more from the calculated trendlines. Additionally, a wider distribution of measurements appeared at lower and intermediate initial bubble-interface distances ($\gamma_0 < 1.5$). This again emphasizes the greater interface influence at lower distances. With decreasing HLB value the concentration of Span 80 in SiOil increases, which proportionally increases the amount of undissolved surfactant. Among the already discussed effects on surface tension, such increasing heterogeneity could influence bubble dynamics. Furthermore, surfactant adsorption at the oil water interface may modify interfacial elasticity during rapid deformation. Variations in Gibbs elasticity [70] could affect the interface's transient “spring-like” resistance during bubble collapse. With this it could influence collapse anisotropy, bubble centroid displacement and jetting [31]. Such effects may become particularly important in the transitional HLB range, where relatively small changes in interfacial properties could greatly affect collapse behaviour.

With changing dimensionless standoff parameter (γ_0), the 4.3 HLB sample (Fig. 5c) demonstrated completely unique bubble collapse dynamics. At γ_0 values above 1.5, bubble displaced away from the oil-water interface during collapse. At these distances bubble collapse occurred comparably to that in systems with the highest HLB values of 15.0 and 12.9, as well as that of dH_2O-SiOil without any surfactant (Fig. 5a). Around $\gamma_0 = 1.5$ bubble displacement distinctly shifted towards the oil-water interface. The same trend in shifting displacement direction has been observed in three experiment repetitions. Additionally, no bubbles trapped at the oil-water interface were observed, which would affect bubble collapse dynamics. This system's collapse dynamics at lower γ_0 have already been discussed in more detail at the end of Section 3.2.

As with systems with intermediate HLB values (Fig. 5b), the heterogeneity of the SiOil phase is increased due to greater amounts of undissolved Span 80. Its effect on bubble collapse dynamics cannot be completely ruled out. Due to the highest Span 80 concentration in this system, a high concentration gradient between the dH_2O and SiOil phase is expected. This could lead to the formation of Marangoni flow [71]. It

could potentially influence the observed phenomena, such as the magnitude of bubble centroid displacement and reversal of jetting direction. Further studies on interfacial rheology are required to fully characterize the potential Marangoni flow and its effects.

The bubble centroid displacement during collapse (L/R_{max}), calculated for each HLB-tailored system, is rearranged and presented in Fig. 6. At each HLB value, bubble displacement has been plotted for dimensionless standoff parameters (γ_0) ranging linearly from 0.1 (red) to 2.0 (blue). Their transparencies increase as γ_0 approaches 1.0. As the system with pure dH_2O and SiOil has no assigned HLB value, these results are not included.

Results reveal a very wide distribution of displacements at the highest HLB values of 15.0 and 12.9. As discussed above, the greater displacements during collapse occur at lower initial bubble-interface distances (opaque red areas in Fig. 6). The distribution of measurements decreases towards 10.7, reaching its minimum at 8.6 and again slightly increasing at 6.4. In this range, bubble displacement becomes weaker and is no longer predominantly negative (oriented away from the interface). At the HLB of 4.3, bubble displacement shifts towards mostly positive values, indicating bubble collapse predominantly towards the oil-water interface. Furthermore, a shift in γ_0 occurs where the lower values (initial distances) again represent greater bubble centroid displacement.

3.4. Static interfacial tension and HLB effect on emulsification

As emulsification is a much slower phenomena compared to cavitation bubble collapse, separate visualization experiments at lower framerates have been conducted. The results for systems with HLB values of 15.0, 8.6 and 4.3 are presented in Fig. 7. The dimensionless standoff parameters (γ_0) for these examples were 0.29, 0.24 and 0.60, respectively. Lower γ_0 have been chosen to maximize cavitation bubble effect on the oil-water interface and consequently the potential for emulsion formation.

Results in Fig. 7a and b show cavitation bubble collapse away from the oil-water interface. During this it partially pulls oil into the water phase, which is visible during the bubble's first rebound (3rd frame) as the uneven droplets surrounding it. As the bubble continues through its following rebound phases, it separates from the cloud of oil droplets and

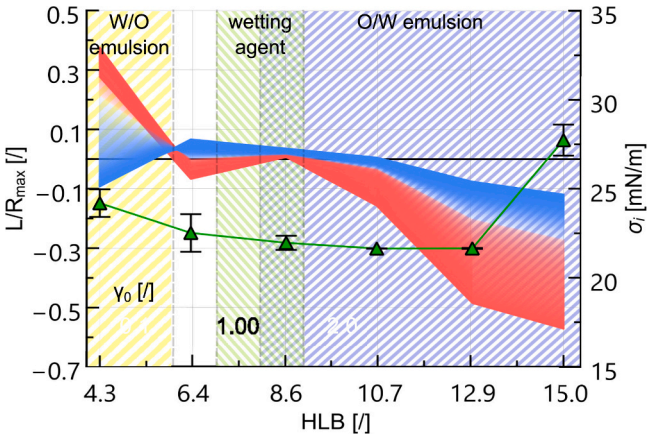

Fig. 6. Cavitation bubble centroid displacement (L/R_{max}) and static oil-water interfacial tension (σ_i, represented by ▲) as an effect of hydrophilic-lipophilic balance (HLB). Displacement is shown at dimensionless standoff parameters (γ_0) ranging from 0.1 (red) to 2.0 (blue). Negative values indicate bubble collapse away from the oil-water interface (and vice versa). The stripped areas represent HLB ranges for typical surfactant applications: water-in-oil (W/O) emulsions (yellow), wetting agents (green) and oil-in-water (O/W) emulsions (blue). (For interpretation of the references to colour in this figure legend, the reader is referred to the web version of this article.)

O/W emulsion becomes clearly visible.

Meanwhile with the bubble collapsing towards the oil-water interface (Fig. 7c), the bubble passes into the oil phase. Due to the great opacity of the oil, the bubble's rebound cycles are not observable. During the later stages (8th frame), however, a cloud of emulsion droplets became visible as it separated from the oil into the water phase. The reader is suggested to consult Supplementary material video S9 for a clearer presentation of the described phenomenon. As proposed by Perdih et al. [17], this indicates firstly the formation of a W/O emulsion, caused by cavitation bubble collapse into the oil phase. The resulting Rayleigh-Taylor instability at the oil-water interface causes parts of the oil phase continuing W/O emulsion to separate into the water phase. This results in the formation of the visible O/W or potentially also W/O/W emulsion. The lack of other components, which could comprise these visible droplets, strongly suggests to them being formed from the SiOil-Span 80 phase. Additionally, their extended stability indicates that they do not represent gas bubbles or remnants of the collapsed cavitation bubble.

The most common HLB ranges for W/O emulsion, wetting agents and O/W emulsions have been marked in Fig. 6 as yellow, green and blue striped areas, respectively. Such comparison visualizes that at HLB values, characteristic for the formation of O/W emulsions (>9), cavitation bubbles were found to predominantly collapse away from the oil-water interface. As the HLB values approach wetting agent ranges (between 7 and 9), the magnitude of cavitation bubbles displacement greatly decreases. Bubble collapse also varies both towards and away from the interface. This indicates the formation of unstable emulsion of both types, a typical characteristic of wetting agents [38]. Additional studies on the bubble dynamics and wetting properties of dH_2O-SiOil systems in this HLB range would need to be conducted to definitively explain their correlation.

Furthermore, the shift in bubble displacement from away to towards the interface occurred inside the HLB range associated with W/O emulsion formation (<6). This indicates that the effect HLB value has on emulsion type and properties is through a change in cavitation bubble collapse dynamics. The magnitude of bubble displacement inside the W/O emulsification range was, however, lower compared to that of O/W emulsification. This could be attributed to the higher oil viscosity, which potentially limits transport phenomena inside the oil phase.

Green triangles in Fig. 6 show the static interfacial tension (σ_i) values of each HLB-tailored oil-water system. The dH_2O-Tween 80 solution with the highest surfactant concentration (at 15.0 HLB) had the lowest surface tension (Fig. 2a). Contrary to previous findings [58], its static interfacial tension with the corresponding SiOil solution (pure oil) measured highest at 27.7 mN m^{-1}. Decreasing HLB (by lowering Tween 80 and increasing Span 80 concentration) led to a sharp decrease in static interfacial tension to 21.6 mN m^{-1}. Thus, it plateaued around the system's optimal HLB value. In addition to having the lowest interfacial tension, a system close to its optimal HLB value also exhibits greatest emulsion stability, smallest average droplet size and highest zeta potential [72]. This is due to the most efficient surfactant molecule arrangement at the interface and consequent interfacial saturation [60]. Further HLB decrease to 4.3 led to a renewed increase in static interfacial tension, peaking at 24.2 mN m^{-1}. A matching relation between HLB value and interfacial tension has previously been observed by Wang et al. [72].

Among the already discussed density and viscosity, surface and interfacial tension also strongly affect bubble collapse dynamics. The surface tension of a liquid influences bubble jetting by affecting the inward pressure of the bubble's surface. Higher surface tension will decrease cavity volume, accelerate collapse and increase jetting force [41–43,73]. However, the trend in surface tension of dH_2O-Tween 80 solutions (Fig. 2a) is not suitably reflected in jetting intensity (Fig. 6). Despite the dH_2O-Tween 80 solution at 15.0 HLB having the lowest surface tension, the bubble displacement in the associated system was highest. This indicates a greater influence of the static oil-water

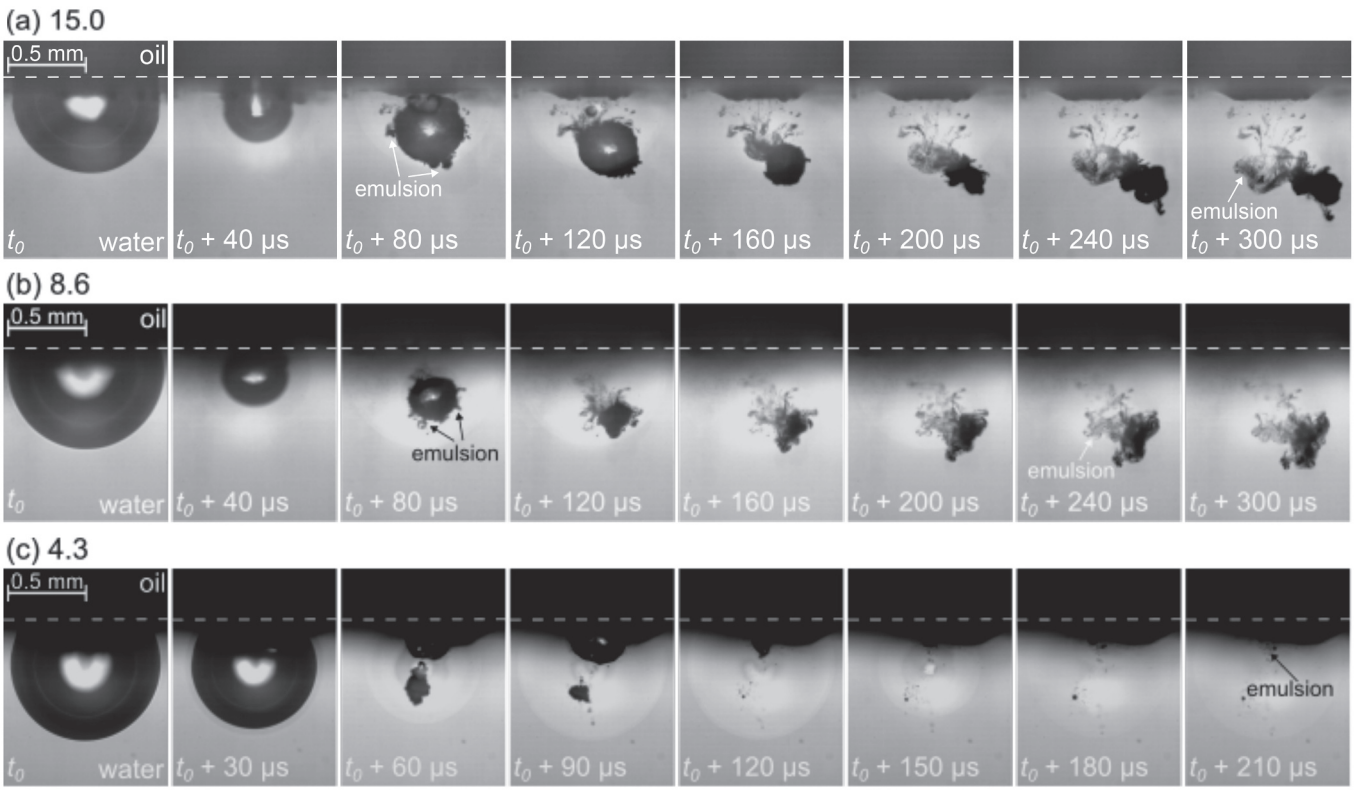

Fig. 7. (videos S7–S9 in Supplementary material): Sequences of cavitation bubble collapse near the oil-water interface demonstrating emulsion formation at different hydrophilic-lipophilic balance (HLB) values: (a) 15.0, (b) 8.6 and (c) 4.3. Their dimensionless standoff parameters (γ_0) were 0.29, 0.24 and 0.60, respectively. The visible bubble artifacts are due to the camera ghosting effect. The white dashed lines represent the respective oil-water interface position. Frames are presented from maximum bubble growth to complete collapse and emulsion formation. Due to the bubble collapse away from the oil-water interface in systems with HLB values of 15.0 and 8.6, oil droplets are pulled into the water phase. Meanwhile, as the bubble jets towards the interface at 4.3, water is moved into the oil phase, which then separates back into the water phase.

interfacial tension than that of individual surface tensions on bubble collapse dynamics.

Similar trends in cavity volume and collapse time at higher surface tensions are also maintained with the bubble collapsing near a neutral wall. Under such conditions, however, bubble collapse velocity will decrease with increasing surface tension [43]. But for a liquid-liquid interface to act comparably to a rigid wall, magnitude higher interfacial tension is required [42]. A deformable interface, on the other hand, can reverse the liquid jet direction [16]. As this is the first research into the influence of HLB value and oil-water interfacial tension on cavitation bubble collapse dynamics, further studies must be conducted in order to thoroughly explain the phenomena.

4. Conclusions

The present study establishes a direct correlation between the hydrophilic-lipophilic balance (HLB) of surfactant systems and cavitation bubble collapse dynamics near a liquid-liquid interface. By systematically tailoring HLB value using surfactants Tween 80 and Span 80, we demonstrate that surfactant-dependent interfacial properties actively determine bubble jetting direction and consequently cavitation-driven emulsification pathways. Due to the technical limitation of being able to form the cavitation bubble exclusively inside the dH_2O-Tween 80 phase, the work's conclusions can perhaps not be generalized to bubble dynamics inside the corresponding SiOil-Span 80 phase. As bubble jetting is strongly dependent on the phase of origin, the precise effects of interfacial parameters on bubble dynamics in such conditions would need to be separately explored. The main findings for bubbe dynamics inside the dH_2O-Tween 80 phase can therefore be summarised as follows:

(1) HLB as an indicator of interfacial cavitation dynamics.

We demonstrate that the system's HLB value indicates the direction and magnitude of bubble jetting. Although parameters such as density and viscosity also influence bubble dynamics [19,26,27,29,40,52], the latter does not change enough to have a noticeable effect [19,52–54]. Meanwhile, the density changes are not significant enough to explain both the variations in the jet's magnitude and the reversal of its direction [14,26,27,29,63]. Bubbles in higher HLB systems ($\geq$ 12.9) follow previously described classical collapse dynamics at liquid-liquid interfaces [21,27,29], where bubbles formed inside the denser liquid jet away from the liquid-liquid interface. Decreasing HLB firstly induces transition to a mixed collapse regime, ultimately leading to a reversal in bubble jetting.

(2) Surfactant modified liquid-liquid interfaces induce jetting reversal.

At low HLB values (4.3) bubble jetting reversed direction towards the interface, despite bubble formation inside the denser phase. This contradicts established density-driven jetting models [16,21] and demonstrates that interfacial physicochemical properties can override classical hydrodynamic predictions. This introduces a new regime of cavitation behaviour governed by interfacial mechanics.

(3) Identification of a transitional bubble dynamics regime potentially linked to wetting conditions.

Intermediate HLB values (between 6.4 and 10.7) exhibit mixed and bidirectional bubble jetting. This aligns closely with HLB ranges of systems associated with wetting agents and colloid science [32,34–36]. Such a potential connection between interfacial wetting behaviour and

cavitation dynamics requires further investigation.

(4) Interfacial tension affects partially the bubble collapse dynamics.

Comparing the present work with prior studies on the effects of viscosity and density [19,52–54] indicates at least a partial influence of the liquid-liquid interfacial tension on bubble dynamics. In the present systems, density variations were found to be >1% for both dH2O-Tween 80 and SiOil-Span 80, and maximum viscosity differences approx. 50% and 13% for dH2O-Tween 80 and SiOil-Span 80, respectively. Furthermore, maximum variations in measured surface tension were approx. 44% for dH2O-Tween 80 and 4% for SiOil-Span 80 solutions.

Although a predominant effect on bubble collapse dynamics might be attributed to interfacial tension, its combined effect with density differences, interfacial structure and surfactant adsorption kinetics cannot be completely ruled out. Future studies would need to be conducted for their clarification, as well as to differentiate between the role of static and dynamic interfacial tension in the observed phenomena. Under such conditions, comparatively small local variations, for example interface structure and positioning, surfactant distribution and bubble shape asymmetry, could produce substantial changes in bubble jetting direction and displacement magnitude.

(5) Mechanistic link between cavitation dynamics and emulsion type.

The direction of bubble jetting directly governs emulsification pathways. Jetting away from the oil-water interface promotes the formation of oil-in-water (O/W) emulsion, while jetting towards the interface primarily produces water-in-oil (W/O) emulsion [16,17]. The experimentally observed HLB ranges for the formation of either emulsion type coincide with HLB ranges for typical surfactant applications [32,34,35]. This provides a physics-based explanation for these empirical guidelines.

The results demonstrate that the HLB value of a surfactant system provides a powerful control parameter for tuning cavitation bubble collapse dynamics and cavitation-driven emulsification processes. It highlights the importance of surfactant's physical properties on emulsion formation mechanisms, which necessitates further studies in order to fully explain its details.

CRediT authorship contribution statement

Žan Boček: Writing – review & editing, Writing – original draft, Visualization, Methodology, Investigation, Formal analysis, Data curation, Conceptualization. **Juan Manuel Rossello:** Writing – review & editing, Writing – original draft, Methodology, Investigation, Formal analysis, Data curation, Conceptualization. **Matevž Dular:** Writing – review & editing, Writing – original draft, Supervision, Resources, Methodology, Funding acquisition, Conceptualization.

Declaration of Competing Interest

The authors declare the following financial interests/personal relationships which may be considered as potential competing interests. Matevz Dular reports financial support was provided by Slovenian Research Agency. If there are other authors, they declare that they have no known competing financial interests or personal relationships that could have appeared to influence the work reported in this paper.

Acknowledgments

The authors declare that they have no competing financial interests or personal relationships that could have influenced the results or interpretation of this work. Additionally, no artificial intelligence (AI) tools were used in data analysis and the preparation or writing of this manuscript.

The authors acknowledge the financial support from the Slovenian Research Agency (Core funding No. P2-0422 and projects: N2-0376 and J2-60032). The authors would like to thank Assist. Prof. Tilen Kopač from the Faculty of Chemistry and Chemical Technology, University of Ljubljana for assistance with viscosity measurements, and Matic Cotič from the Faculty of Mechanical Engineering, University of Ljubljana for assistance with surface and interfacial tension measurements. Additionally, the authors would like to thank Mitja Kostelec from the National Institute of Chemistry Slovenia for assistance in figure preparation.

Appendix A. Supplementary data

Supplementary data to this article can be found online at https://doi.org/10.1016/j.jcis.2026.141209.

Data availability

Data will be made available on request.

References

[1] T.F. Tadros, Emulsion Science and Technology: A General Introduction, in: Emulsion Science and Technology, 2009, pp. 1–56, https://doi.org/10.1002/9783527626564.ch1.
[2] T. Tadros, P. Izquierdo, J. Esquena, C. Solans, Formation and stability of nanoemulsions, Adv. Colloid Interf. Sci. 108–109 (2004) 303–318, https://doi.org/10.1016/j.cis.2003.10.023.
[3] T. Panagiotou, R. Fisher, Improving product quality with entrapped stable emulsions: from theory to industrial application, Challenges 3 (2012) 84–113, https://doi.org/10.3390/challe3020084.
[4] A.K.D. Santhi, S. Sureshkumar, Factors influencing meat emulsion properties and product texture: a review, Crit. Rev. Food Sci. Nutr. 57 (2017) 2021–2027, https://doi.org/10.1080/10408398.2013.858027.
[5] D.W. Stanley, H.D. Goff, A.K. Smith, Texture-Structure Relationships in Foamed Dairy Emulsions, 1996.
[6] C. Chung, D.J. McClements, Structure-function relationships in food emulsions: improving food quality and sensory perception, Food Struct. 1 (2014) 106–126, https://doi.org/10.1016/j.foostr.2013.11.002.
[7] T. Mahmood, N. Akhtar, S. Manickam, Interfacial film stabilized W/O/W nano multiple emulsions loaded with green tea and lotus extracts: systematic characterization of physicochemical properties and shelf-storage stability, J. Nanobiotechnol. 12 (2014), https://doi.org/10.1186/1477-3155-12-20.
[8] S.Y. Tang, M. Sivakumar, Design and evaluation of aspirin-loaded water-in-oil-in-water submicron multiple emulsions generated using two-stage ultrasonic cavitational emulsification technique, Asia Pac. J. Chem. Eng. 7 (2012) S145–S156, https://doi.org/10.1002/apj.664.
[9] S.Y. Tang, P. Shridharan, M. Sivakumar, Impact of process parameters in the generation of novel aspirin nanoemulsions - comparative studies between ultrasound cavitation and microfluidizer, Ultrason. Sonochem. 20 (2013) 485–497, https://doi.org/10.1016/j.ultsonch.2012.04.005.
[10] B. Mishra, B.L. Sahoo, M. Mishra, D. Shukla, V. Kumar, Design of a controlled release liquid formulation of lamotrigine, Daru 19 (2011) 126–137.
[11] C. Tan, D.J. McClements, Application of advanced emulsion technology in the food industry: a review and critical evaluation, Foods 10 (2021), https://doi.org/10.3390/foods10040812.
[12] J.M. Gutiérrez, C. González, A. Maestro, I. Solè, C.M. Pey, J. Nolla, Nanoemulsions: new applications and optimization of their preparation, Curr. Opin. Colloid Interface Sci. 13 (2008) 245–251, https://doi.org/10.1016/j.cocis.2008.01.005.
[13] J. Carpenter, V.K. Saharan, Ultrasonic assisted formation and stability of mustard oil in water nanoemulsion: effect of process parameters and their optimization, Ultrason. Sonochem. 35 (2017) 422–430, https://doi.org/10.1016/j.ultsonch.2016.10.021.
[14] W. Lauterborn, T. Kurz, Physics of bubble oscillations, Rep. Prog. Phys. 73 (2010), https://doi.org/10.1088/0034-4885/73/10/106501.
[15] C. Cogné, S. Laboureт, R. Peczalski, O. Louisnard, F. Baillon, F. Espitalier, Theoretical model of ice nucleation induced by acoustic cavitation. Part 1: pressure and temperature profiles around a single bubble, Ultrason. Sonochem. 29 (2016) 447–454, https://doi.org/10.1016/j.ultsonch.2015.05.038.
[16] T. Yamamoto, S.V. Komarov, Liquid jet directionality and droplet behavior during emulsification of two liquids due to acoustic cavitation, Ultrason. Sonochem. 62 (2020), https://doi.org/10.1016/j.ultsonch.2019.104874.
[17] T. Stepišnik Perdih, M. Zupanc, M. Dular, Revision of the mechanisms behind oil-water (O/W) emulsion preparation by ultrasound and cavitation, Ultrason. Sonochem. 51 (2019) 298–304, https://doi.org/10.1016/j.ultsonch.2018.10.003.
[18] W.H. Wu, D.G. Eskin, A. Priyadarshi, T. Subroto, I. Tzanakis, W. Zhai, New insights into the mechanisms of ultrasonic emulsification in the oil–water system and the

role of gas bubbles, Ultrason. Sonochem. 73 (2021), https://doi.org/10.1016/j.ultsonch.2021.105501.
[19] Y. Liu, Z.Y. Zheng, Z.B. He, T.B. Zeng, W.H. Cai, H. Qi, Influence of liquid viscosity on the interactions between cavitation bubbles and flat liquid-liquid interfaces, J. Hydrodyn. 36 (2024) 1057–1072, https://doi.org/10.1007/s42241-025-0113-3.
[20] K. Ashoke Raman, J. Manuel Rosselló, H. Reese, C.-D. Ohl, Microemulsification from single laser-induced cavitation bubbles, J. Fluid Mech. 953 (2022) A27, https://doi.org/10.1017/jfm.2022.971.
[21] R. Han, A.M. Zhang, S. Tan, S. Li, Interaction of cavitation bubbles with the interface of two immiscible fluids on multiple time scales, J. Fluid Mech. 932 (2022), https://doi.org/10.1017/jfm.2021.976.
[22] A. Bußmann, F. Riahi, B. Gökce, S. Adami, S. Barcikowski, N.A. Adams, Investigation of cavitation bubble dynamics near a solid wall by high-resolution numerical simulation, Phys. Fluids 35 (2023), https://doi.org/10.1063/5.0135924.
[23] A. Pearson, E. Cox, J.R. Blake, S.R. Otto, Bubble interactions near a free surface, Eng. Anal. Bound. Elem. 28 (2004) 295–313, https://doi.org/10.1016/S0955-7997(03)00079-1.
[24] J.M. Rosselló, H. Reese, C.-D. Ohl, Dynamics of pulsed laser-induced cavities on a liquid–gas interface: from a conical splash to a 'bullet' jet, J. Fluid Mech. 939 (2022) A35, https://doi.org/10.1017/jfm.2022.223.
[25] J.M. Rosselló, H. Reese, K.A. Raman, C.-D. Ohl, Bubble nucleation and jetting inside a millimetric droplet, J. Fluid Mech. 968 (2023) A19, https://doi.org/10.1017/jfm.2023.542.
[26] T. Yamamoto, R. Matsutaka, S.V. Komarov, High-speed imaging of ultrasonic emulsification using a water-gallium system, Ultrason. Sonochem. 71 (2021), https://doi.org/10.1016/j.ultsonch.2020.105387.
[27] U. Orthaber, M. Dular, R. Petkovšek, Characterization of jet parameters related to cavitation bubble dynamics in a vicinity of a flat liquid-liquid interface, Exp. Thermal Fluid Sci. 136 (2022), https://doi.org/10.1016/j.expthermflusci.2022.110651.
[28] Z. Ren, H. Han, H. Zeng, C. Sun, Y. Tagawa, Z. Zuo, S. Liu, Interactions of a collapsing laser-induced cavitation bubble with a hemispherical droplet attached to a rigid boundary, 2023, https://doi.org/10.48550/arXiv.2304.01533.
[29] U. Orthaber, J. Zevnik, R. Petkovšek, M. Dular, Cavitation bubble collapse in a vicinity of a liquid-liquid interface – basic research into emulsification process, Ultrason. Sonochem. 68 (2020), https://doi.org/10.1016/j.ultsonch.2020.105224.
[30] Z. Yin, Z. Huang, C. Tu, X. Gao, F. Bao, Dynamic characteristics of bubble collapse near the liquid-liquid interface, Water 12 (2020), https://doi.org/10.3390/w12102794.
[31] A.M. Luz, G. Barbosa, C. Manske, F.W. Tavares, Tween-80 on water/oil Interface: structure and interfacial tension by molecular dynamics simulations, Langmuir 39 (2023) 3255–3265, https://doi.org/10.1021/acs.langmuir.2c03001.
[32] I. Kralova, J. Sjöblom, Surfactants used in food industry: a review, J. Dispers. Sci. Technol. 30 (2009) 1363–1383, https://doi.org/10.1080/01932690902735561.
[33] R. Pichot, F. Spyropoulos, I.T. Norton, O/W emulsions stabilised by both low molecular weight surfactants and colloidal particles: the effect of surfactant type and concentration, J. Colloid Interface Sci. 352 (2010) 128–135, https://doi.org/10.1016/j.jcis.2010.08.021.
[34] M.A. Bos, T. van Vliet, Interfacial rheological properties of adsorbed protein layers and surfactants: a review, Adv. Colloid Interf. Sci. 91 (2001) 437–471, https://doi.org/10.1016/S0001-8686(00)00077-4.
[35] W.C. Griffin, Classification of surface active agents by "HLB", J. Cosmet. Sci. 1 (1946) 311–326, https://api.semanticscholar.org/CorpusID:138032744 (accessed January 28, 2026).
[36] T. Schmidts, D. Dobler, A.-C. Guldan, N. Paulus, F. Runkel, Multiple W/O/W emulsions—using the required HLB for emulsifier evaluation, Colloids Surf. A Physicochem. Eng. Asp. 372 (2010) 48–54, https://doi.org/10.1016/j.colsurfa.2010.09.025.
[37] Inamuddin, C.O. Adetunji, Applications of Next Generation Biosurfactants in the Food Sector, Academic Press, 2023, https://doi.org/10.1016/C2019-0-05486-6.
[38] S.A. Abdelaziz, E.M. Ahmed, M. Sadek, Synthesis of homologous series of surfactants from renewable resources, structure–properties relationship, surface active performance, evaluation of their antimicrobial and anticancer potentialities, Sci. Rep. 14 (2024), https://doi.org/10.1038/s41598-024-62905-3.
[39] A. Ashok N, M. Sontakke, Plant-based emulsifiers: sources, extraction, properties and applications, Pharm. Innov. 12 (2023) 08–16, https://doi.org/10.22271/tpi.2023.v12.i5a.20043.
[40] W. Yang, J. Ouyang, Y. Meng, T. Tang, J. Chen, B. Han, Effect of superplasticizer and wetting agent on volumetric and mechanical properties of cold recycled mixture with asphalt emulsion, Adv. Mater. Sci. Eng. (2020), https://doi.org/10.1155/2020/6251653, 2020.
[41] X.M. Liu, J. He, J. Lu, X.W. Ni, Effect of surface tension on a liquid-jet produced by the collapse of a laser-induced bubble against a rigid boundary, Opt. Laser Technol. 41 (2009) 21–24, https://doi.org/10.1016/j.optlastec.2008.04.006.
[42] E. Samiei, M. Shams, R. Ebrahimi, A novel numerical scheme for the investigation of surface tension effects on growth and collapse stages of cavitation bubbles, European Journal of Mechanics, B/Fluids 30 (2011) 41–50, https://doi.org/10.1016/j.euromechflu.2010.09.002.
[43] Y. Wang, H. Peng, X. He, J. Zhang, Cavitation bubbles with a tunable-surface-tension thermal lattice Boltzmann model, Phys. Fluids 34 (2022), https://doi.org/10.1063/5.0113500.
[44] G. Smejkal, V. Gross, A. Lazarev, Theoretical and experimental determinations of the hydrophilic–lipophilic balance (HLB) of representative oils and lecithins, Colloids Interfaces 8 (2024) 21, https://doi.org/10.3390/colloids8020021.
[45] I.K. Hong, S.I. Kim, S.B. Lee, Effects of HLB value on oil-in-water emulsions: droplet size, rheological behavior, zeta-potential, and creaming index, J. Ind. Eng. Chem. 67 (2018) 123–131, https://doi.org/10.1016/J.JIEC.2018.06.022.
[46] P.H. Tsai, T. Kurniawan, A.B. Wang, A simple technique to achieve meniscus-free interfaces, Phys. Fluids 31 (2019), https://doi.org/10.1063/1.5080659.
[47] O. Supponen, D. Obreschkow, M. Tinguely, P. Kobel, N. Dorsaz, M. Farhat, Scaling laws for jets of single cavitation bubbles, J. Fluid Mech. 802 (2016) 263–293, https://doi.org/10.1017/jfm.2016.463.
[48] K. Szymczyk, A. Taraba, Aggregation behavior of Triton X-114 and tween 80 at various temperatures and concentrations studied by density and viscosity measurements, J. Therm. Anal. Calorim. 126 (2016) 315–326, https://doi.org/10.1007/s10973-016-5631-3.
[49] K. Szymczyk, M. Szaniawska, A. Taraba, Micellar parameters of aqueous solutions of tween 20 and 60 at different temperatures: volumetric and viscometric study, Colloids Interfaces 2 (2018), https://doi.org/10.3390/colloids2030034.
[50] A.S. Al-Janabi, M. Hussin, M.Z. Abdullah, Stability, thermal conductivity and rheological properties of graphene and MWCNT in nanolubricant using additive surfactants, Case Stud. Therm. Eng. 28 (2021), https://doi.org/10.1016/j.csite.2021.101607.
[51] Xuefan Gu, L. Gao, Y. Li, S. Chen, J. Zhang, W. Du, C. Qu, G. Chen, Performance and mechanism of span surfactants as clean flow improvers for crude oil, Pet. Chem. 60 (2020) 140–145, https://doi.org/10.1134/S0965544120010156.
[52] Y. Shen, K. Yasui, T. Zhu, M. Ashokkumar, A model for the effect of bulk liquid viscosity on cavitation bubble dynamics, Phys. Chem. Chem. Phys. 19 (2017) 20635–20640, https://doi.org/10.1039/C7CP03194G.
[53] J. Luo, G. Fu, W. Xu, Y. Zhai, L. Bai, J. Li, T. Qu, Experimental study on attenuation effect of liquid viscosity on shockwaves of cavitation bubbles collapse, Ultrason. Sonochem. 111 (2024), https://doi.org/10.1016/j.ultsonch.2024.107063.
[54] J.T. Feng, J.H. Xing, S.P. Wang, Y.L. Liu, H. Tang, A.M. Zhang, Investigation on the cavitation bubble dynamics and pressure characteristics near a wall with a viscous oil layer, J. Fluid Mech. 1014 (2025), https://doi.org/10.1017/jfm.2025.10180.
[55] A. Taraba, K. Szymczyk, A. Zdziennicka, B. Jańczuk, Mutual influence of some flavonoids and classical nonionic surfactants on their adsorption and volumetric properties at different temperatures, Molecules 27 (2022), https://doi.org/10.3390/molecules27092842.
[56] K. Lunkenheimer, A. Lind, M. Jost, Surface tension of surfactant solutions, J. Phys. Chem. B 107 (2003) 7527–7531, https://doi.org/10.1021/jp0224867.
[57] A. Bąk, W. Podgórska, Interfacial and surface tensions of toluene/water and air/water systems with nonionic surfactants tween 20 and tween 80, Colloids Surf. A Physicochem. Eng. Asp. 504 (2016) 414–425, https://doi.org/10.1016/j.colsurfa.2016.05.091.
[58] X. Tang, K.J. Huston, R.G. Larson, Molecular dynamics simulations of structure-property relationships of tween 80 surfactants in water and at interfaces, J. Phys. Chem. B 118 (2014) 12907–12918, https://doi.org/10.1021/jp507499k.
[59] Z. Yan, Y. Tian, J. Hu, Z. Yao, G.G. Fuller, Revising HLB theory for surface tension prediction of the aqueous solution of asphalt emulsifiers, Colloids Surf. A Physicochem. Eng. Asp. 715 (2025), https://doi.org/10.1016/j.colsurfa.2025.136663.
[60] X. Jiang, M. Liu, X. Li, L. Wang, S. Liang, X. Guo, Effects of surfactant and hydrophobic nanoparticles on the crude oil-water interfacial tension, Energies 14 (2021), https://doi.org/10.3390/en14196234.
[61] F.O. Opawale, D.J. Burgess, Influence of interfacial properties of lipophilic surfactants on water-in-oil emulsion stability, J. Colloid Interface Sci. (1998), https://doi.org/10.1006/jcis.1997.5222.
[62] G. Gutiérrez, J.M. Benito, J. Coca, C. Pazos, Evaporation of aqueous dispersed systems and concentrated emulsions formulated with non-ionic surfactants, Int. J. Heat Mass Transf. 69 (2014) 117–128, https://doi.org/10.1016/j.ijheatmasstransfer.2013.10.013.
[63] S.W. Ohl, E. Klaseboer, B.C. Khoo, The dynamics of a non-equilibrium bubble near bio-materials, Phys. Med. Biol. 54 (2009) 6313–6336, https://doi.org/10.1088/0031-9155/54/20/019.
[64] Y. Zhong, Y. Zhao, X. Gao, F. Bao, Experimental study on interaction between a cavitation bubble and an oil layer-water interface, AIP Adv. 14 (2024), https://doi.org/10.1063/5.0211208.
[65] Y. Zhou, S. Zhang, Z. Wu, P. Cui, Experimental study of a cavitation bubble impacting an oil-covered free surface, AIP Adv. 15 (2025), https://doi.org/10.1063/5.0284626.
[66] J.M. Rosselló, H.P. Hoeppe, M. Koch, C. Lechner, M. Osterhoff, M. Vassholz, J. Hagemann, J. Möller, M. Scholz, U. Boesenberg, J. Hallmann, C. Kim, A. Zozulya, W. Lu, R. Shayduk, A. Madsen, T. Salditt, R. Mettin, Jetting bubbles observed by x-ray holography at a free-electron laser: internal structure and the effect of non-axisymmetric boundary conditions, Exp. Fluids 65 (2024) 20, https://doi.org/10.1007/s00348-023-03759-9.
[67] C. Li, Z. Mei, Q. Liu, J. Wang, J. Xu, D. Sun, Formation and properties of paraffin wax submicron emulsions prepared by the emulsion inversion point method, Colloids Surf. A Physicochem. Eng. Asp. 356 (2010) 71–77, https://doi.org/10.1016/j.colsurfa.2009.12.036.
[68] M. Dular, C.D. Ohl, Bulk material influence on the aggressiveness of cavitation – questioning the microjet impact influence and suggesting a possible way to erosion mitigation, Wear 530–531 (2023) 205061, https://doi.org/10.1016/j.wear.2023.205061.
[69] J.C. Adamowski, F. Buiochi, C. Simon, E.C.N. Silva, R.A. Sigelmann, Ultrasonic measurement of density of liquids, J. Acoust. Soc. Am. 97 (1995) 354–361, https://doi.org/10.1121/1.412320.

[70] P. Marmottant, S. Hilgenfeldt, Controlled vesicle deformation and lysis by single oscillating bubbles, Nature 423 (2003) 153–156, https://doi.org/10.1038/nature01613.
[71] A. Nikkhah, S. Shin, Marangoni flows triggered by cationic-anionic surfactant complexation, J. Colloid Interface Sci. 676 (2024) 168–176, https://doi.org/10.1016/J.JCIS.2024.07.014.
[72] Q. Wang, H. Zhang, Y. Han, Y. Cui, X. Han, Study on the relationships between the oil HLB value and emulsion stabilization, RSC Adv. 13 (2023) 24692–24698, https://doi.org/10.1039/d3ra04592g.
[73] A.N. Sabzeghabae, L.F. Devia-Cruz, E. Gutierrez-Herrera, S. Camacho-Lopez, G. Aguilar, Bubble dynamics of laser-induced cavitation in plasmonic gold nanorod solutions and the relative effect of surface tension and viscosity, Opt. Laser Technol. 134 (2021), https://doi.org/10.1016/j.optlastec.2020.106621.